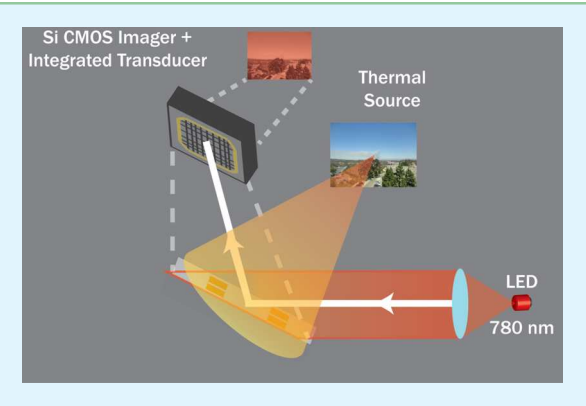


Simple Nanoimprinted Polymer Nanostructures for Uncooled Thermal Detection by Direct Surface Plasmon Resonance Imaging

Brandon Hong,*,[†] Felipe Vallini,[†] Cheng-Yi Fang,^{‡‡} Amr Alasaad,[‡] and Yeshaiahu Fainman[†]

Supporting Information

ABSTRACT: We experimentally demonstrate the uncooled detection of long wavelength infrared (IR) radiation by thermal surface plasmon sensing using an all optical readout format. Thermal infrared radiation absorbed by an IR-sensitive material with high thermo-optic coefficient coated on a metal grating creates a refractive index change detectable by the shift of the supported surface plasmon resonance (SPR) measured optically in the visible spectrum. The interface localization of SPR modes and optical readout allow for submicrometer thin film transducers and eliminate complex readout integrated circuits, respectively, reducing form factor, leveraging robust visible detectors, and enabling low-cost imaging cameras. We experimentally present the radiative heat induced thermo-optic action detectable by SPR shift through imaging of a thermal source onto a bulk metal grating substrate with IR-absorptive



silicon nitride coating. Toward focal plane array integration, a route to facile fabrication of pixelated metal grating structures by nanoimprint lithography is developed, where a stable polymer, parylene-C, serves as an IR-absorptive layer with a high thermooptic coefficient. Experimental detection of IR radiation from real thermal sources imaged at infinity is demonstrated by our nanoimprinted polymer-SPR pixels with an estimated noise equivalent temperature difference of 21.9 K.

KEYWORDS: uncooled infrared detection, thermo-optic effect, surface plasmon resonance, nanoimprint, parylene, surface plasmon resonance imaging

INTRODUCTION

The infrared (IR) optical spectrum offers unique access to physical processes otherwise invisible to the naked eye. Measurements in this band have proven fruitful in their diverse applications, including the acquisition of characteristic chemical vibrational spectra for scientific and medical analysis, optical data transfer and telecommunications, and thermal imaging for military and civil service. 1-6 With thermal IR radiation emitted by many terrestrial objects centered in the $8-14~\mu m$ band as gray body radiators (objects with imperfect blackbody emissivity), detection and imaging within this spectral band is fundamental to remote sensing in low-light or obfuscating environmental conditions. Since their conception, IR detector sensitivity, bandwidth, and form factor have been improved tremendously, fast, sensitive, and affordable IR imagers are becoming increasingly market-competitive.8

Many mechanisms for IR detection have been explored and characterized. Photon detectors based on both intrinsic and extrinsic band gap carrier generation have been wellcharacterized as IR detectors and focal plane arrays with high sensitivity. 1,8,9 However, their performance is contingent upon low device temperatures maintained by cryogenic cooling, rendering such detectors inseparable from accompanying refrigeration units. Thermal IR sensors leveraging thermoelectric, pyroelectric, and bolometric effects have been developed and have enjoyed significant commercial success. 10 By the absorption of incident radiation, thermal detectors measure the effect of induced temperature shift by voltage generation against a junction thermal reference (thermoelectric effect), induced ferroelectric voltage (pyroelectric effect), or a thermal shift of electrical resistance (bolometric effect). Generally, performance in these detector elements is limited by their heat transfer characteristics, which affect the specific detectivity¹¹ and time response of the developed thermal sensor. Consequently, a drawback for thermal sensors is the high thermal conductance of silicon upon the readout integrated circuit (ROIC) that limits the maximum temperature contrast achievable, where contact to the ROIC substrate must

Received: November 3, 2016 Accepted: January 26, 2017 Published: January 26, 2017

[†]Ultrafast and Nanoscale Optics, Department of Electrical Engineering, University of California, San Diego, California 92093, United

^{‡‡}Ultrafast and Nanoscale Optics, Department of Materials Science & Engineering, University of California, San Diego, California 92093, United States

^{*}Center of Excellence for Telecommunication King Abdulaziz City for Science and Technology, Riyadh 12371, Saudi Arabia

be limited by employing multistep etch processes to suspend the sensing thermal element by narrow legs which also function as electrical leads for sensing.¹

A solution to this issue is developing thermal IR sensing based on the temperature induced change of the material optical properties to leverage the improvements made in the sensitivity of optical detection technologies. Crucially, thermooptic IR sensors employ an optical readout system and do not require integrated design of a thermal focal plane array into a ROIC substrate plane. Sensors based on MEMS bimorphs, 11-13 photonic crystals, 14 bioinspired reflectors, 15 low dimensional materials such as graphene, 16 and integrated optical components¹⁷ have been investigated. A significant advantage claimed for optical readout in thermo-optic IR sensing is the dispensation of a ROIC, minimizing or completely eliminating the need for electrical contact.¹⁸ Readout mechanisms can be made independent of the substrate, conferring a design freedom for thermal isolation unique to a ROIC-independent platform, also enabling parallelism provided by imaging over the sensor array.

Besides thermal management and parallelism, the absorption of existing thermal detectors have been enhanced through plasmonics; 19,20 by resonantly interacting with a metallic nanostructure, the incident infrared radiation is more strongly absorbed to the near-field, thereby improving the efficiency of the absorption cross-section for the infrared sensor architecture. While plasmonic devices have been employed to improve light collection efficiency, it is well-known that plasmonic modes are sensitive to the thermo-optic properties of the dielectric interface in which the mode is supported. ^{21,22} Surface plasmon resonance (SPR) sensing confers a narrow Lorentzian-shape resonance 23,24 for highly sensitive resonance shift detection that is uniquely sensitive to refractive index changes in low dimensional film profiles owing to its evanescent transverse mode profile. This modality has enjoyed significant success in biosensing, with high sensitivity to refractive index changes in nanometer-scale biofilms and protein interactions and the capability for highly parallel and real-time grid readout as an optical imaging modality. 25-27 Transitively, the localized sensitivity of SPR is highly amenable to the detection of IR induced thermo-optic changes in the local refractive index of thin IR sensitive films.²⁰

In this manuscript, we experimentally demonstrate the uncooled detection of long-wave infrared (LWIR) radiation by thermal surface plasmon sensing, using an all optical readout format. The SPRs are employed to detect the IR induced temperature change, leveraging the high sensitivity of the tightly bound mode profile to refractive index changes in a lowprofile thermal mass. By depositing a thermal IR sensitive material onto a metallic grating, IR induced temperature changes in the refractive index via the thermo-optic coefficient are then measured as shifts in the SPRs. A demonstration of the thermo-optic shift is first presented as a response to the absorption of thermal infrared light in a glassy silicon nitride layer as a proof of concept. We then change from a continuous grating to discrete and spatially resolvable SPR grating pixels of $500 \times 500 \ \mu \text{m}^2$ area fabricated by nanoimprint lithography for IR detection by SPR imaging. After the thermo-optic action of IR absorption in the dielectric cladding on SPR was demonstrated, polymer parylene-C was chosen as the grating pixel cladding layer for its high thermo-optic coefficient. Thermal IR detection in SPR imaging was experimentally measured with two thermal sources of different temperatures to

extrapolate a system limit of detection. Design outlooks for performance based on pixel delimitation are also presented toward affordable room temperature high sensitivity thermal detection.

THEORY

Surface Plasmon Polariton Resonance. A surface plasmon polariton (SPP) is an electromagnetic surface wave phenomenon that can be described as the resonant oscillation of charge density bound to the interface of a charge carrier-rich material such as a metal or semiconductor and dielectric layer whose real part of dielectric functions have different signs. The modal structure of SPP resonances is characterized by high field densities propagating along the interface and exponential decay of the field strength in the direction normal to the interface. Physically, the resonance frequency is determined by the intrinsic plasma frequency and damping frequencies of the metal and the effective dielectric constant of the layer over which the evanescent tail persists. Importantly, SPP resonances are supported only for transverse magnetic (TM) waves, wherein the modal electric field lies in the plane spanned by the surface normal and direction of resonant propagation; no analogous mode is supported in the perpendicular polarization.

As a propagating electromagnetic wave, Maxwell's equations can be solved to yield a dispersion relation for SPPs of a TM polarized wave supported by a single nonmagnetic dielectric—metal interface:

$$k_{\rm SPP} = k_{\rm o} \sqrt{\frac{\epsilon_{\rm d} \epsilon_{\rm m}}{\epsilon_{\rm d} + \epsilon_{\rm m}}} \tag{1}$$

where $\epsilon_{\rm d}$ and $\epsilon_{\rm m}$ are the relative permittivities of the dielectric and

metal materials, respectively, and k_o is the free-space wavenumber defined as $k_o = \frac{\omega}{c_o}$ where ω is the oscillatory frequency and c_o is the speed of light in vacuum. For most metals in the visible frequency, the large negativity of the real part of the relative permittivity results in the SPP wavenumber exceeding the free-space wavenumber. Optical excitation of the SPP is thus possible through momentum matching schemes that evanescently couple into the guided mode. A common method for coupling to the poor field is through subvayable and matching

SPP wavenumber exceeding the free-space wavenumber. Optical excitation of the SPP is thus possible through momentum matching schemes that evanescently couple into the guided mode. A common method for coupling to the near-field is through subwavelength grating couplers, wherein metallic films have been patterned into or upon periodically nanostructured films that diffract incident light into nonpropagating evanescent modes which couple into the propagating plasmonic modes. ^{29,23} For a square one-dimensional periodic metallic grating, the accessible diffraction orders described by the grating equation can be used to excite the SPP momentum $k_{\rm SPP}$:

$$k_{\rm o} \sin \theta_{\rm i} + m K_{\rm G} = k_{\rm SPP} \tag{2}$$

where $\theta_{\rm i}$ is the angle of incidence with respect to the surface normal, m is an integer diffraction order, and $K_{\rm G} = \frac{2\pi}{\Lambda}$ is the grating wavenumber, where Λ is the grating periodicity. For grating periodicities smaller than the incidence wavelength, only the zeroth specular reflection order exists, allowing for efficient coupling into the guided SPP upon phase matching. Moreover, sufficiently subwavelength grating periodicity imparts considerable momentum to the projected wavevector such that small angles can be used to excite the SPP. In general, coupling efficiency is highly dependent on the material stack and unit cell geometry of the grating; for square gratings, SPP coupling efficiency can be tuned by varying the depth contrast of the grating. For our device, a grating coupler is employed to provide small interior optical readout path angles for coupling and imaging.

Thermal Properties. Fundamentally, thermal infrared detection can be described as the measurable increase in temperature of a thermal mass due to the absorption of radiant infrared energy. The one-dimensional heat conductance equation describes the temperature dynamics of a thermal mass in response to the continuous absorption of thermal radiation:

$$C\frac{\mathrm{d}T}{\mathrm{d}t} + GT = \alpha P(t) \tag{3}$$

where *T* is the temperature over time of the thermal slab, *C* is the slab heat capacity, G is the heat conductance connecting the slab to an environmental heat sink, and α describes the fractional power absorbed from incident radiant flux P(t) under the assumption of ideal slab emissivity. 1,10 When a shutter is opened to expose the thermal mass to the radiant flux from a thermal source, the intercepted exitance can be expressed as $P(t) = P_0 u(t)$, where u(t) is the unit step function and P_0 is the steady state radiant exitance. The temperature step response is then $T(t) = T_o(1 - e^{-t/\tau})$, where $\tau = C/G$ is the characteristic time constant and $T_0 = \alpha P_0/G$ is the steady state temperature; the step response to a closing shutter is linearly related and can be similarly derived. It can then be understood that for sensitive and fast thermal infrared detectors, excellent thermal insulation by materials with low thermal conductivity is necessary for large temperature contrast, while small element sizes with low specific heat capacity maintain short time constants.

RESULTS AND DISCUSSION

Thermo-Optic IR Sensing. An experimental setup was devised to observe the thermo-optic shift in the surface plasmon resonance induced by optical absorption in a bulk infrared absorbing dielectric cladding, according to the general principle of thermo-optic readout in Figure 1a. Of particular interest was the evaluation of the first-order temperature step response to the radiative heat transfer from a thermal infrared source, and characterization of the optical readout sensitivity of an SPP resonance shift in the visible domain. The measurement setup consists of two independent optical paths for respective infrared thermal sensing and optical readout, as seen in Figure 1b. To demonstrate the collection of IR emission from a thermal source, a silicon nitride furnace igniter at 1300 °C is imaged by a ZnSe f/2.3 optic with f = 6.24 cm (Umicore) in a 2f system (relay) configuration onto the SPR supporting grating device at an angle of approximately 20° from the surface normal. A reflective metallic shutter is placed between the optic and the source to regulate the thermal infrared flux from the source to substrate. The visible spectrum optical readout originates from a fiber coupled broadband tungsten lamp source of unpolarized white light that is subsequently collimated and polarized in the plane of incidence, spanned by the grating surface and normal to the grating wavevector, for TM polarization. The polarized light is incident upon the SPR grating at an angle of approximately 10° with respect to the grating surface normal. At the fixed incidence angle, select bands within the collimated broadband source that scatter from the grating are resonantly phase-matched to the SPR mode and absorbed. Nonresonantly reflected probe light then passes through the remaining optical path by a series of mirrors and into a Thorlabs reflective fiber collimator, which couples the signal to a UV-NIR spectrometer (Ocean Optics HR2000 UV-NIR).

To fabricate the plasmonic IR sensing device illustrated in the inset of Figure 1b, an AZ1505 photoresist layer is spun onto a silicon substrate to a 400 nm thickness, UV holographically exposed, and developed into quasi-sinusoidal grating with 570 nm periodicity, followed by sputtering of 5 nm of adhesion titanium and 75 nm of gold (Denton Discovery 18). The fabrication procedure for the metallized gratings employs similar methods and instrumentation as previously reported.31,32 An IR absorbing layer is developed by sputtering 200 nm of silicon nitride (Si₃N₄) onto the SPP grating layers; IR absorption in the thermal $8-14 \mu m$ spectral band is verified by Fourier transform infrared (FTIR) spectroscopic measurement in attenuated total internal reflection (ATR) (Thermo-

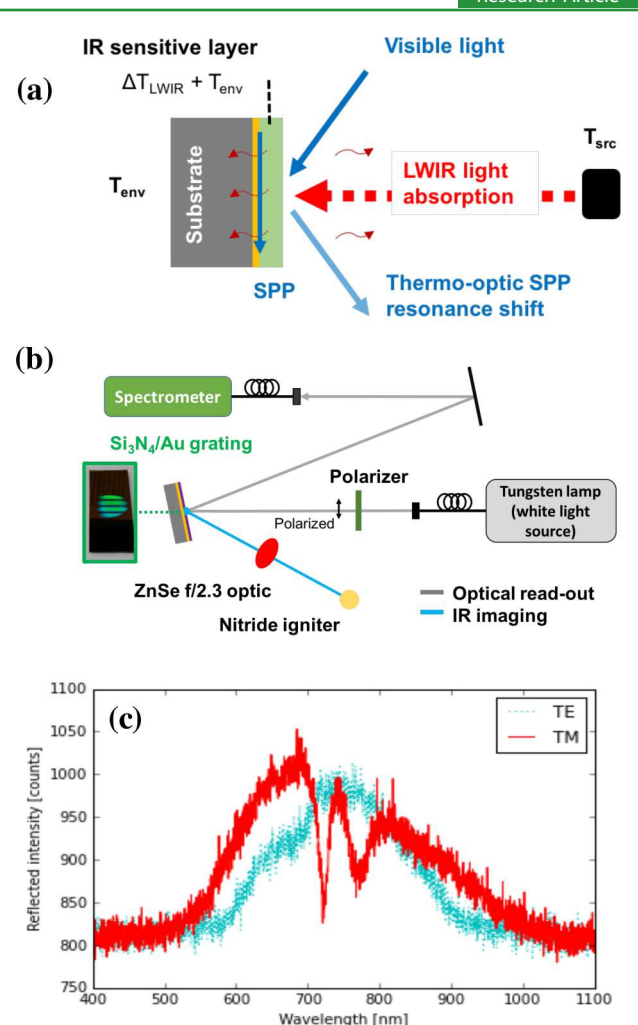


Figure 1. Thermo-optic detection of LWIR radiation measures temperature dependent visible light transmission or reflection from an IR absorbing system (a). For SPR, the resonance shift induced by an IR absorbing dielectric interface can be resolved spectrally or angularly. The temperature difference ΔT_{LWIR} is maintained by thermal isolation where heat is lost to environment $T_{\rm env}$ by substrate conduction and the radiative background. Measurement setup (b) with thermal imaging relay system (blue) and visible readout optical components (gray). Both paths are coincident upon an IR sensitive silicon nitride thin film which is patterned onto a holographically exposed, developed, and metallized grating as the device under test (DUT, see Supporting Information, Figure 2 for implemented setup). As in panel c, light polarized in the plane of incidence (transverse magnetic, TM) couples into surface plasmon polaritons (SPP), while light polarized perpendicularly (transverse electric, TE) does not couple. Two resonant absorptions are visible, indicating that multiple grating orders satisfy the grating assisted phase matching for SPR excitation.

Fisher Nicolet). By ellipsometric measurement, the refractive index of the silicon nitride layer was measured to be approximately 1.91 for 632.8 nm wavelength light.

Figure 1c shows the reflected intensity for TM and TE polarizations. Because the incidence angle of the readout light is fixed in this configuration, refractive index changes in the absorbing layer are detected as spectral shifts of the resonant band owing to changes in the phase matching condition at the fixed angle. In spectral readout generalized to Figure 1a, the use of broadband SPP resonance interrogation provides a large dynamic range defined by spectrometer and source spectral **ACS Applied Materials & Interfaces**

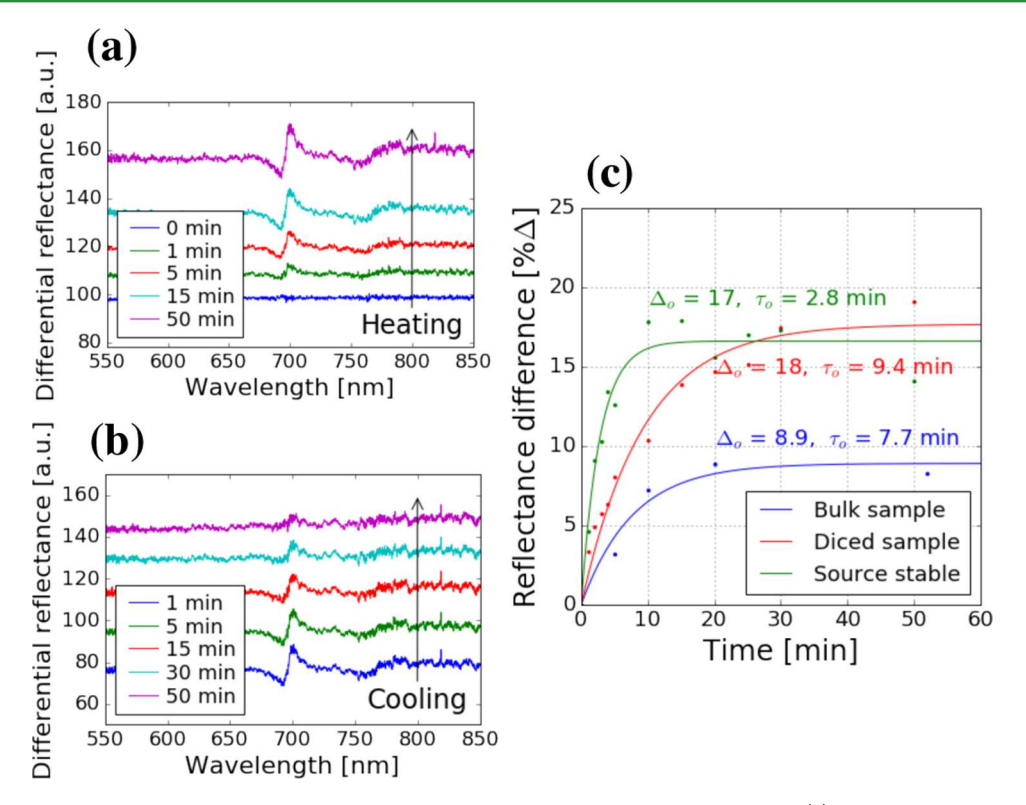


Figure 2. Thermo-optic SPP resonance blue-shift induced by absorption of IR light from thermal source (a) and red-shift toward the baseline after shutter closure (b). This spectral shift is differentially observed by subtracting the measured baseline resonance spectrum from the shifted spectra; greater spectral shift results in less overlap and higher peak contrast. For a blue-shifted resonance, the differential spectrum minimum is present in wavelengths shorter than the peak wavelength of the subtracted baseline resonance. Upon cooling, the shifted spectrum red-shifts toward baseline conditions, and the peak contrast diminishes as the cooling spectrum overlaps the baseline. (c) Time response of the SPP sensor on a bulk substrate and for an identical sensor diced to the dimensions of the imaged source such that the imaged radiant exitance is closely matched to the delimited sensor dimension. For the delimited sensor (red), a significant increase in the steady state thermal shift is observed compared to the bulk sensor (blue), indicative of a decrease in the thermal heat conductance, while the proportionally smaller increase in the time constant owes to the reduced size of the film as well as the smaller heat capacity. The characteristic time constant of the detector is measured upon opening the shutter after heating the thermal source to its steady state (green).

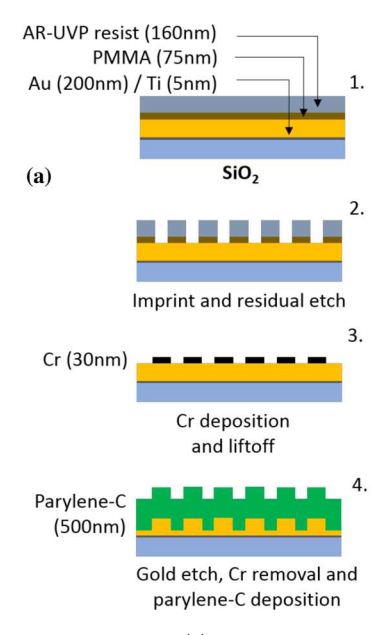
range,²³ allowing for the fixed setup to accommodate the selection of IR sensitive materials with different refractive indices without experimental setup variation. For the silicon nitride film refractive index, the grating eq 2 can be solved to show that, at the fixed incidence angle, the positive second order evanescent diffraction mode is phase matched to the SPP resonance. Hence, increases in the dielectric refractive index serve to blue-shift the spectral SPR resonance.

Optical paths for thermal infrared signal and visible optical readout were made coincident onto the SPR sensor area by aligning the visible image of the thermal source and the readout light onto the same area. As the thermal radiation was incident upon the sensor substrate at a more extreme angle, detectable scatter radiation did not couple into the visible readout path. This independence was verified by continuous spectrometer readings without the readout beam with source alternately shuttered and exposed and without detectable perturbation to the measured readout spectrum.

Upon thermal IR absorption by the transducer silicon nitride film, the surface plasmon resonance spectral peak could be observed to shift, indicating a refractive index change due to the heating in the infrared absorbing nitride cladding film. The shift was quantified by taking a baseline spectrum with the thermal source removed and subtracting it from subsequently obtained spectra over time; the absolute difference in the two peaks of maximum and minimum spectral intensity represents the

differential shift in the surface plasmon resonance, similar to a previously described method (see Supporting Information for a more detailed description of the method).³³ As the sensor substrate is exposed to the thermal source, the imaged infrared radiation is absorbed by the SPP resonance-supporting dielectric layer, inducing heating at the interface and throughout the bulk film. This temperature increase can be observed in Figure 2a as a blue-shift in resonance coupling wavelength, indicative of a positive thermo-optic effect in the dielectric interface coefficient ϵ_1 as dictated by both SPP resonance and momentum matching eqs 2 and 3. Similarly, switching off the thermal source results in a decrease in radiant flux upon the sensor, and a cooling red-shift can be observed in Figure 2b as the source and substrate thermalize to the environment. Illustrated in Figure 2c, the characteristic first order time response to heating can be observed. After a period of sustained exposure to the thermal source, the spectral blueshift of the resonant input wavelength was observed to asymptotically cease; the equilibrium spectral shift from the baseline and rise time then characterize the substrate for the imaged source.

For each bulk and diced sample, the thermal source was brought from room temperature to steady state with the shutter open and imaged continuously onto the detector substrate. Compared with the sensor on the bulk substrate, the diced sample showed a significantly larger thermo-optic shift (blue



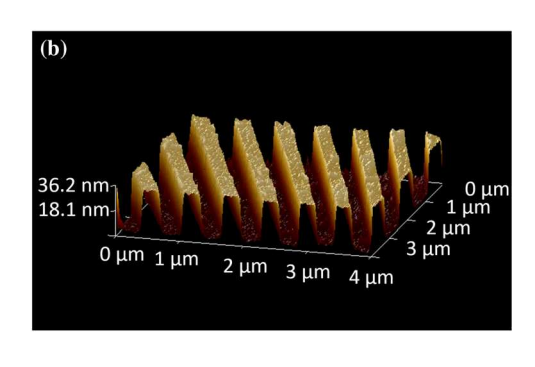


Figure 3. Nanoimprint fabrication process (a) begins with a Au-metallized borosilicate substrate for the spinning (1) and imprinting (2) of a bilayer AR-UVP/PMMA polymer stack. Cr mask transfer by liftoff (3) is performed for direct RIE etching into the gold for (4) subsequent deposition of 500 nm IR sensitive parylene-C in a furnace. (b) The gold film grating has a 600 nm periodicity with 30 nm depth modulation and 50% duty cycle, as measured by AFM.

and red curves in Figure 2c). Because the imaged source occupies only a fraction of the area of the bulk sample, delimiting the sensor area to dimensions that fall within the bounds of the thermal source image significantly reduces the heat conductance to the substrate while retaining the net radiant exitance delivered to the substrate; pursuant to eq 3, this yields a larger thermo-optic shift. While the reduced thermal contact to the mount generally yields a larger time constant, the sensor delimitation also decreases the heat capacity of the silicon nitride film, and only a 22% increase in the time constant is observed. Finally, the rise time of the igniter thermal source itself was accounted for by allowing the source to ramp for 10 min with the shutter closed and subsequently opening the shutter for imaging. Measuring the diced sensor response, the time constant, now restricted to the intrinsic device properties, is reduced by a factor of 2.75, from 9.4 to 2.8 min, shown in the green curve of Figure 2c.

Thermal IR SPR-Imaging. Having demonstrated the SPP resonance sensitivity to thermal infrared absorption, a method for multiplex division was sought. A well-reported advantage of optical readout of IR detection is the parallelism afforded by imaging the sensor array.³⁴ By imaging the thermal source onto the sensitive image plane, the spatial distribution of the infrared radiance imaged across the array can be detected as the effects of localized heat transfer on the optical properties of the imager, as measured by a probing light source. In particular, when an SPP resonance supporting substrate is illuminated by a probe beam fixed in incidence near the resonant coupling angle for the corresponding wavelength, the image in reflection shows significant attenuation of light in regions of SPP resonance coupling as compared to images at nonresonant angles; refractive index changes in the dielectric support that shift the coupling angle are measured as intensity shifts. This technique, known as surface plasmon resonance imaging, is routinely employed for the readout of immunoassays in biosensing in which highly multiplexed sites for binding kinetics must be rapidly observed in parallel.³⁴

Toward SPR resonance imaging, individual sensing sites as a pixelation of the SPP resonant grating sensor were developed. Formatted as pixelated elements, lateral design of the patterning provides control over heat capacity and conductance to maximize the signal for individual resolution elements as well as control over the minimization of thermal cross-talk between pixels. As the SPP resonant grating coupler requires subwavelength resolution in fabrication as well as the available throughput to pattern in an array format, it is desirable to employ a fabrication process that allows for large scale patterning with high resolution. A candidate for these criteria is nanoimprint lithography, where a high resolution mold of the desired negative pattern is impressed upon a thermo- or photocurable plastic film which can be removed upon curing to contain the designed pattern. When the resist is hosted by a wafer substrate, traditional liftoff and etch steps can be subsequently performed upon the imprinted pattern, allowing for transfer of the pattern into the substrate itself. This technique achieves resolution scales comparable to those of electron-beam lithography and can repeatedly transfer patterns from an electron-beam resolution mold to entire wafers, amenable for rapid large scale patterning.

A nanoimprint process was developed for the thermal-IR SPP resonant sensor pixels. The substrate used was prime grade borosilicate glass; the choice of glass lowers the substrate conductivity compared to that of silicon substrates, an advantage to be claimed by forgoing electrical ROIC. The substrate, with roughness <5 nm across, was solvent cleaned, and a sequential 5 nm Ti adhesion layer and 200 nm Au film was evaporated by electron-beam evaporation onto the substrate for the eventual patterning of the supporting gold gratings (Temescal BJD 1800). The substrate was then spin-coated with 75 nm of PMMA with a 90 s soft bake at 180 °C and 160 nm of AR-UVP imprint resist (Figure 3a-1). An electron-beam patterned master mold with a 500 × 500 μ m² area of a one-dimensional SiO₂ grating with 1 μ m depth and 600 nm periodicity with 50% duty cycle was fabricated and

transferred to a secondary polymeric stamp for imprinting into the imprint resist. The stamp was imprinted into the resist by hard contact through nanoimprint lithography tooling (EVG aligner) and subsequently reactive ion etched (RIE) using CF₄ and oxygen gases for respective top layer residue etch and PMMA under layer etch with the top layer acting as a polymeric mask (Oxford RIE P80) (Figure 3a-2). Following this step, 30 nm of Cr was deposited by electron-beam metal evaporation, and immersion in acetone for liftoff was performed (Figure 3a-3). With the Cr pattern as an etch mask, RIE etch was directly performed into the gold using a CHF₃ gas. Finally, the Cr etch mask was removed by Cr etchant, which was measured to be highly selective against Au and its adhesion layer owing to the conformality of the Au film. Etch modulation depth of 30 nm into the gold and periodicity of 600 nm with 50% duty cycle was verified by AFM measurements (Figure

Because the detector sensitivity is dependent on the magnitude of refractive index shift in the dielectric per unit temperature shift generated by thermal infrared absorption, a higher thermo-optic coefficient (TOC) was desired for the IR absorption dielectric layer (Figure 3a-4). Polymers have been reported for high coefficients of linear thermal expansion compared to glassy materials and possess comparably higher thermo-optic shifts.³⁵ Parylene-C is a polymer known for its mechanical, thermal, and chemical stability, used often as a protective coating for antifouling and biocompatibility applications with excellent longevity. 36,37 Such a material is desirable as a dielectric layer that can repeatedly transduce small temperature changes through IR absorption without suffering lifetime drift in the base refractive index or sensitivity degradation by hardening. With the reported linear coefficient of thermal expansion to be $3.5 \times 10^{-5} \text{ K}^{-1}$, an empirical formula was used to calculate the TOC for parylene-C to be -6.3×10^{-5} RIU °C^{1-,35} about 2.5 higher than reported measurements of silicon nitride thermo-optic coefficient of 2.5 × 10⁻⁵ RIU °C^{1-.38} Figure 4 shows the FTIR spectroscopy analysis of parylene-C with absorption bands in the 7–14 μ m region conducive to transduce the absorption of thermal IR light to thermo-optic shifts measurable by SPP resonance. Having characterized the IR absorptivity of parylene-C in the band of interest, a parylene coater system (SDS PDS2010) at 15 mTorr chamber pressure was used to vaporize 1 g of parylene-C dimer at 50 °C, converted into monomer by pyrolysis at 550 °C and polymerized onto the fabricated SPR grating-pixel for a conformal 530 nm parylene-C thin film (Figure 3a, step 4).

To measure the imprinted IR sensitive SPP resonant pixels developed by SPR imaging, a quasi-monochromatic collimated LED source centered at 780 nm illuminates the grating at a fixed angle of 24° with respect to the sensor surface normal and is polarized in the plane of incidence as a TM wave (Figure 5a). While the resonance angle can be calculated to be at 26.5°, the implemented angle is slightly offset to maximize the shift contrast dynamic range (i.e., biased at the maximum line shape slope). In reflection, a CMOS camera (eCon See3Cam 12CU-NIR) and f=7.5 cm optic images the grating pixel. For the thermal source, a separate arm is angled at approximately 45°, and a $7-12~\mu{\rm m}$ antireflection coated Ge filter is placed to block out Si detector sensitive bands in the visible spectrum below 1.975 $\mu{\rm m}$ emitted from the thermal source that might contaminate the sensor signal and provide a window for the

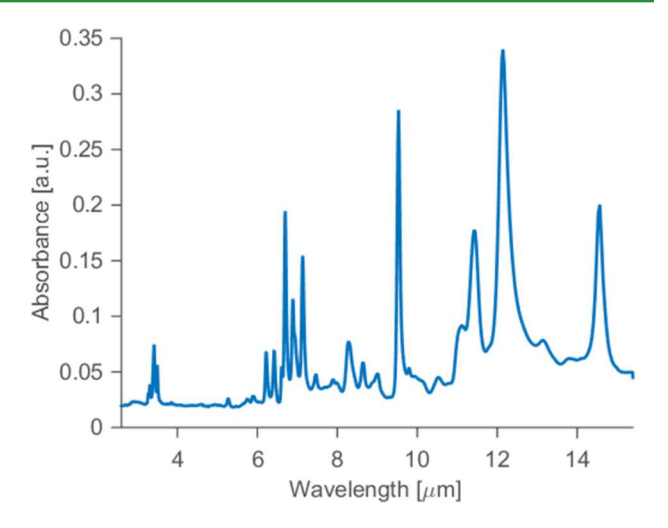


Figure 4. FTIR spectroscopy of parylene-C was conducted in attenuated total internal reflection (ATR) mode. Strong absorption bands can be seen in the $8-14~\mu m$ spectral band, amenable for thermal infrared detection. In conjunction with a high thermo-optic coefficient and intrinsic thermal stability, the thermal band absorptivity of parylene-C functions as the IR sensitive layer for SPR imaging. Strong bands also exist in the extended $6-8~\mu m$ region, allowing for higher temperature sources centered in this region to maintain high signal contrast with limited saturation effects.

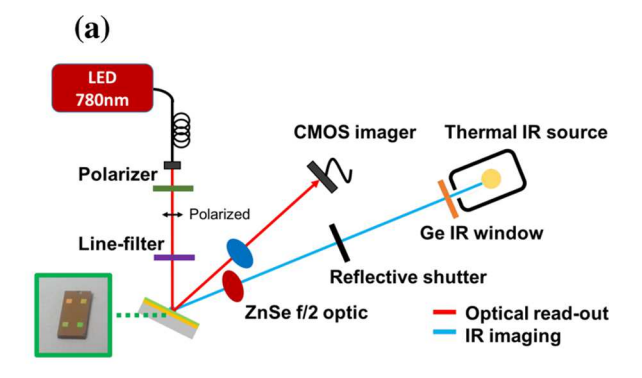
8–14 μ m thermal IR band. The thermal source is imaged from infinity onto the pixel by an f/2 ZnSe optic.

Two heating elements were used as thermal sources: in addition to the nitride igniter previously described at approximately 1600 K, a soldering iron measured by thermocouple to be 423 K was also imaged. While optically shuttered, the sources are allowed to reach thermal equilibrium as the optical readout system obtains a baseline to acquire the sensor noise figure σ , the standard deviation. With a sufficient 1 min baseline at 20 fps averaged to 0.33 Hz sample acquisition, the shutter is opened, and the measured intensity responses are fit well to a first order differential equation time response. Shown in Figure 5b, the signal response is normalized to the 3σ according to the obtained baseline, termed 1 response unit (RU); the sensor measures the igniter response to be approximately 26 RU, and the solder iron response is measured to be approximately 3 RU. The fit extrapolated rise time constant is 31 s with similar agreement for the fall time.

A plot showing the additional increase in thermal radiance of an object over 293 K emitting in the $8-14 \mu m$ band is shown in Figure 6, and the measured thermal sources are plotted according to a unity emissivity. Because nonunity emissivities emit lower spectral radiance, the band radiance from an ideal blackbody at the same temperature is greater than or equivalent to the nonideal radiance. Thus, the calculation based on ideal emissivity presents an upper bound on the radiance emitted by an object at the same temperature, and transitively, an upper bound on the noise equivalent temperature difference (NETD). The NETD is the temperature difference between an object and the background necessary to induce a variation in the detector equal to its noise, i.e., 1σ . In our device, the temperature difference in the imaged source compared to its background required to induce a 0.33 RU sensor response can be extrapolated to be NETD = 21.9 K.

Improvements upon the time constant are desirable, and the effects of lateral thermal isolation for the pixel on the sensor heat capacity were investigated. To implement this isolation,

ACS Applied Materials & Interfaces



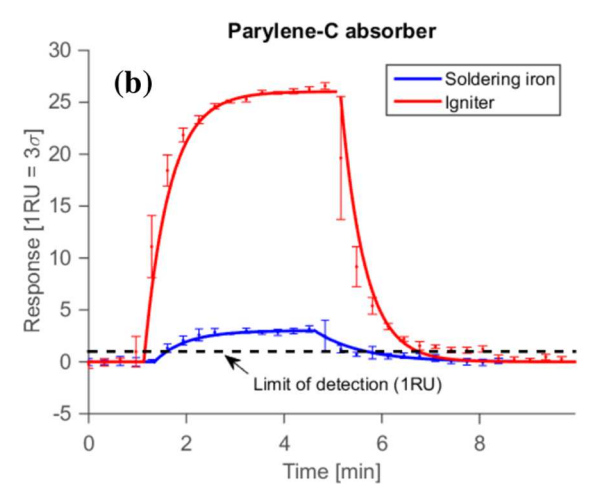


Figure 5. Measurement setup for SPP resonance imaging detection of a thermal source (a) consists of an infrared imaging path (blue) and a visible readout path (red) with the two paths coincident on the polymeric grating sensor (green). A thermal IR source reflective housing is passed through a Ge window that filters out light below 1.975 μ m and is imaged from infinity onto the device under test. The readout arm begins with a collimated LED centered at 780 nm, which is polarized in the plane of incidence and line-filtered for a 5 nm bandwidth, incident on the DUT at 24.5° from the surface normal; the reflection is imaged onto the CMOS imager (see Supporting Information, Figure 3 for implemented setup). The absorption by a single $500 \times 500 \ \mu \text{m}^2$ SPP resonant pixel is measured (b) in real time, and any background fluctuations of the source are removed by a nonresonant control region. Approximately 1 min of closed shutter baseline is acquired for characterizing noise figures, and the shutter is subsequently opened until steady state is reached, at which point the shutter is closed and the DUT temperature returns to baseline. Intensity units are normalized by the measured baseline noise power σ to response units such that 1 RU = 3σ . A soldering iron at 423 K and a nitride igniter at 1600 K are measured.

approximately 0.5 μ m wide and 1 μ m deep trenches were milled by focused Ga ion beam along the 500 \times 500 μ m perimeter of the pixel (FEI Scios DualBeam), as shown in Figure 7a. Imaging the nitride igniter upon this modified sample, the characteristic time constant was shown to decrease by a factor of \sim 2 upon the pixel delimitation (Figure 7b). When delimitations were set, the heat capacity was restricted to the delimited pixel area in addition to a restriction on the lateral heat conductance to nonresonant areas outside the grating pixel dimensions, leading to a slight rise in the signal response and a larger decrease in the device time response. Similar to isolation techniques employed in bolometer design, simple etch steps incorporated into grating pixel fabrication for the thermal-IR SPR sensor can serve to control and improve the detector time

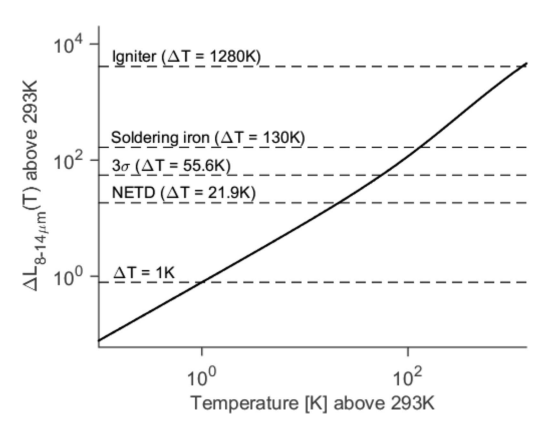


Figure 6. For ideal radiators above room temperature, the net band radiance difference in the 8–14 μ m band over a 293 K blackbody is calculated from the Planck law spectral distribution. The differential radiance for the thermal sources measured are charted, and on the basis of the detected thermal signal from the T=423 K soldering iron source, the noise equivalent temperature difference was calculated as 21.9 K, the object temperature with the proportional spectral radiance to induce a measured noise equivalent to 0.33 RU (or σ) signal response.

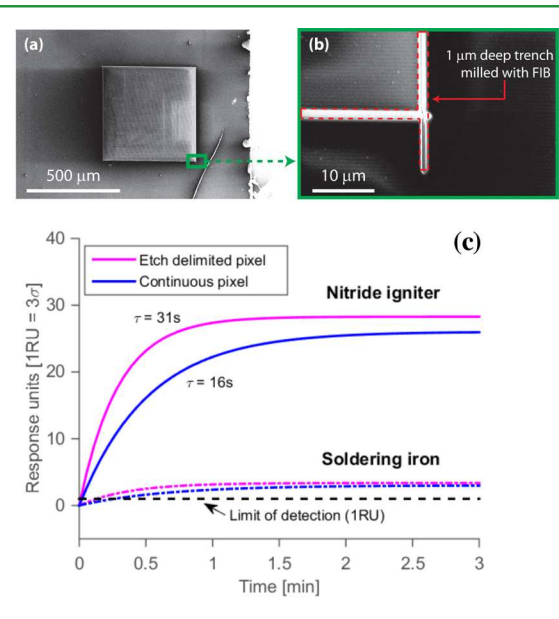


Figure 7. Focused ion beam etching about the perimeter of the 500 \times 500 μm^2 thermal IR SPP resonant grating pixel (a) limits lateral heat conductance from the heated pixel; etched trenches are marked in red. For an approximately 1 μm etch depth by FIB milling (b), a characteristic time response of 16 s was observed for the limit of detection, and a 1.93 factor decrease in the characteristic time response was observed (c).

response and signal-to-noise ratio (SNR). This demonstration shows that the response time can be dramatically improved with careful consideration to the pixel size and delimitation toward thermal isolation.

CONCLUSION

A thermal infrared detection platform based on SPR imaging was fabricated and measured. Nanoimprint lithography was used to generate SPP resonant sensor elements in pixel format, and parylene was demonstrated in its capacity as a thermo-optic polymer. An inexpensive CMOS imager and LED were employed to acquire readout of the thermal shift by SPR

imaging. Through this system, characteristic sensitivity and response times of the SPR thermal imaging sensor were experimentally characterized, and delimitation of the pixel was shown to be a design element capable of improving response time.

ASSOCIATED CONTENT

Supporting Information

The Supporting Information is available free of charge on the ACS Publications website at DOI: 10.1021/acsami.6b14054.

Detailed description of the differential spectrum measurement used as a method for detecting SPR shifts and pictures of the implemented experimental setup illustrated in Figures 1b and 5a (PDF)

AUTHOR INFORMATION

Corresponding Author

*E-mail: bjhong@eng.ucsd.edu.

ORCID

Brandon Hong: 0000-0002-4800-1040

Funding

This work was supported by the National Science Foundation (NSF), the NSF Center for Integrated Access Networks, the Office of Naval Research Multi- Disciplinary Research Initiative, the Defense Advanced Research Projects Agency (DARPA), the Cymer Corporation, King Abdul Aziz City for Science and Technology under the nanophotonics project, and the National Science, Technology and Innovation Plan (NSTIP), Grant 34-989. The work was performed in part at the San Diego Nanotechnology Infrastructure, a member of the National Nanotechnology Coordinated Infrastructure, which is supported by the National Science Foundation (ECCS- 1542148).

Notes

The authors declare no competing financial interest.

ACKNOWLEDGMENTS

Lindsay Freeman for AFM measurements and Vinod Krishnamoorthy for helping develop the surface plasmon resonance measurement computer interface are acknowledged.

ABBREVIATIONS

SPR, surface plasmon resonance SPP, surface plasmon polariton LWIR, long wave infrared

REFERENCES

- (1) Vollmer, M.; Möllmann, K.-P. Infrared Thermal Imaging: Fundamentals, Research and Applications; John Wiley & Sons: Hoboken, NJ, 2010.
- (2) Ring, E. F. J.; Ammer, K. Infrared Thermal Imaging in Medicine. *Physiol. Meas.* **2012**, 33 (3), R33.
- (3) Balaras, C. A.; Argiriou, A. A. Infrared Thermography for Building Diagnostics. *Energy Build.* **2002**, 34 (2), 171–183.
- (4) Robinson, J. M. Fire from Space: Global Fire Evaluation Using Infrared Remote Sensing. *Int. J. Remote Sens.* **1991**, *12* (1), 3–24.
- (5) Yariv, A.; Yeh, P. Photonics: Optical Electronics in Modern Communications (the Oxford Series in Electrical and Computer Engineering); Oxford University Press, Inc.: Oxford, 2006.
- (6) Nezhad, M. P.; Simic, A.; Bondarenko, O.; Slutsky, B.; Mizrahi, A.; Feng, L.; Lomakin, V.; Fainman, Y. Room-Temperature Subwavelength Metallo-Dielectric Lasers. *Nat. Photonics* **2010**, *4* (6), 395–399.

- (7) Holst, G. C. Common Sense Approach to Thermal Imaging; SPIE Optical Engineering Press: Washington, D.C., 2000.
- (8) Rogalski, A. Recent Progress in Infrared Detector Technologies. Infrared Phys. Technol. 2011, 54 (3), 136-154.
- (9) Rogalski, A. Infrared Detectors: Status and Trends. *Prog. Quantum Electron.* **2003**, 27 (2), 59–210.
- (10) Kruse, P. W. Uncooled Thermal Imaging: Arrays, Systems, and Applications; SPIE Press: Bellingham, WA, 2001; Vol. 2003.
- (11) Jones, C. D. W.; Bolle, C. A.; Ryf, R.; Simon, M. E.; Pardo, F.; Aksyuk, V. A.; Lai, W.-C.; Bower, J. E.; Miner, J. F.; Klemens, F. P.; Cirelli, R. A. MEMS Thermal Imager with Optical Readout. *Sens. Actuators, A* **2009**, *155* (1), 47–57.
- (12) Toy, M. F.; Ferhanoglu, O.; Torun, H.; Urey, H. Uncooled Infrared Thermo-Mechanical Detector Array: Design, Fabrication and Testing. *Sens. Actuators, A* **2009**, *156* (1), 88–94.
- (13) Senesac, L. R.; Corbeil, J. L.; Rajic, S.; Lavrik, N. V.; Datskos, P. G. IR Imaging Using Uncooled Microcantilever Detectors. *Ultramicroscopy* **2003**, *97* (1), 451–458.
- (14) Exner, A. T.; Pavlichenko, I.; Lotsch, B. V.; Scarpa, G.; Lugli, P. Low-Cost Thermo-Optic Imaging Sensors: A Detection Principle Based on Tunable One-Dimensional Photonic Crystals. *ACS Appl. Mater. Interfaces* **2013**, *5* (5), 1575–1582.
- (15) Pris, A. D.; Utturkar, Y.; Surman, C.; Morris, W. G.; Vert, A.; Zalyubovskiy, S.; Deng, T.; Ghiradella, H. T.; Potyrailo, R. A. Towards High-Speed Imaging of Infrared Photons with Bio-Inspired Nanoarchitectures. *Nat. Photonics* **2012**, *6* (3), 195–200.
- (16) Qian, Z.; Hui, Y.; Liu, F.; Kang, S.; Kar, S.; Rinaldi, M. Graphene—aluminum Nitride NEMS Resonant Infrared Detector. *Microsyst. Nanoeng.* **2016**, *2*, 1.
- (17) Zhu, J.; Ozdemir, S. K.; Yang, L. Infrared Light Detection Using a Whispering-Gallery-Mode Optical Microcavity. *Appl. Phys. Lett.* **2014**, *104* (17), 171114.
- (18) Ostrower, D. Optical Thermal Imaging—replacing Microbolometer Technology and Achieving Universal Deployment. *III-Vs Rev.* **2006**, *19* (6), 24–27.
- (19) Zhu, H.; Yi, F.; Cubukcu, E. Nanoantenna Absorbers for Thermal Detectors. *IEEE Photonics Technol. Lett.* **2012**, 24 (14), 1194–1196.
- (20) Yi, F.; Zhu, H.; Reed, J. C.; Zhu, A. Y.; Cubukcu, E. Thermoplasmonic Membrane-Based Infrared Detector. *IEEE Photonics Technol. Lett.* **2014**, *26* (2), 202–205.
- (21) Turhan-Sayan, G. Temperature Effects on Surface Plasmon Resonance: Design Considerations for an Optical Temperature Sensor. *J. Lightwave Technol.* **2003**, 21 (3), 805.
- (22) Chiang, H. P.; Chen, C.-W.; Wu, J. J.; Li, H. L.; Lin, T. Y.; Sánchez, E. J.; Leung, P. T. Effects of Temperature on the Surface Plasmon Resonance at a Metal—semiconductor Interface. *Thin Solid Films* **2007**, *515* (17), 6953–6961.
- (23) Pang, L.; Hwang, G. M.; Slutsky, B.; Fainman, Y. Spectral Sensitivity of Two-Dimensional Nanohole Array Surface Plasmon Polariton Resonance Sensor. *Appl. Phys. Lett.* **2007**, *91* (12), 123112.
- (24) Tetz, K. A.; Pang, L.; Fainman, Y. High-Resolution Surface Plasmon Resonance Sensor Based on Linewidth-Optimized Nanohole Array Transmittance. *Opt. Lett.* **2006**, *31* (10), 1528–1530.
- (25) Homola, J.; Yee, S. S.; Gauglitz, G. Surface Plasmon Resonance Sensors: Review. Sens. Actuators, B 1999, 54 (1), 3–15.
- (26) Homola, J. Present and Future of Surface Plasmon Resonance Biosensors. *Anal. Bioanal. Chem.* **2003**, 377 (3), 528–39.
- (27) Hwang, G. M.; Pang, L.; Mullen, E. H.; Fainman, Y. Plasmonic Sensing of Biological Analytes Through Nanoholes. *IEEE Sens. J.* **2008**, 8 (12), 2074–2079.
- (28) Raether, H. Surface Plasmons on Rough and Smooth Surfaces and on Gratings, 1st ed; Springer-Verlag: Berlin, 1988.
- (29) Dostálek, J.; Homola, J. Surface Plasmon Resonance Sensor Based on an Array of Diffraction Gratings for Highly Parallelized Observation of Biomolecular Interactions. *Sens. Actuators, B* **2008**, *129* (1), 303–310.
- (30) Chen, H. M.; Pang, L.; Kher, A.; Fainman, Y. Three-Dimensional Composite Metallodielectric Nanostructure for En-

- hanced Surface Plasmon Resonance Sensing. Appl. Phys. Lett. 2009, 94 (7), 73117.
- (31) Hong, B.; Sun, A.; Pang, L.; Venkatesh, A. G.; Hall, D.; Fainman, Y. Integration of Faradaic Electrochemical Impedance Spectroscopy into a Scalable Surface Plasmon Biosensor for in Tandem Detection. *Opt. Express* **2015**, 23 (23), 30237–30249.
- (32) Pang, L.; Nakagawa, W.; Fainman, Y. Fabrication of Optical Structures Using SU-8 Photoresist and Chemically Assisted Ion Beam Etching. *Opt. Eng.* **2003**, 42 (10), 2912–2917.
- (33) Ptasinski, J.; Pang, L.; Sun, P.-C.; Slutsky, B.; Fainman, Y. Differential Detection for Nanoplasmonic Resonance Sensors. *IEEE Sens. J.* **2012**, *12* (2), 384–388.
- (34) Wong, C. L.; Olivo, M. Surface Plasmon Resonance Imaging Sensors: A Review. *Plasmonics* **2014**, *9* (4), 809–824.
- (35) Zhang, Z.; Zhao, P.; Lin, P.; Sun, F. Thermo-Optic Coefficients of Polymers for Optical Waveguide Applications. *Polymer* **2006**, *47* (14), 4893–4896.
- (36) Loeb, G. E.; Bak, M. J.; Salcman, M.; Schmidt, E. M. Parylene as a Chronically Stable, Reproducible Microelectrode Insulator. *IEEE Trans. Biomed. Eng.* **1977**, *24*, 121–128.
- (37) Shin, Y. S.; Cho, K.; Lim, S. H.; Chung, S.; Park, S.-J.; Chung, C.; Han, D.-C.; Chang, J. K. PDMS-Based Micro PCR Chip with Parylene Coating. *J. Micromech. Microeng.* **2003**, *13* (5), 768.
- (38) Arbabi, A.; Goddard, L. L. Measurements of the Refractive Indices and Thermo-Optic Coefficients of Si 3 N 4 and SiO X Using Microring Resonances. *Opt. Lett.* **2013**, 38 (19), 3878–3881.